Journal of Engineering Science and Technology
Vol. 14, No. 5 (2019) 2964 - 2978

VALIDATION OF RESIDUAL STRESS DISTRIBUTIONS IN MULTIPASS DISSIMILAR JOINTS FOR GTAW PROCESS

HARINADH VEMANABOINA[1,*], G. EDISON[1], SURESH AKELLA[2]

[1]SMEC, VIT University, Vellore, Tamilnadu, India
[2]Sreyas Institute of Engineering and Technology, Nagole, Hyderabad-500068, India
*Corresponding Author: harinadh.vh@gmail.com

Abstract

Dissimilar metals joining has shown precise interest in recent decades due to the stringent fabrication requirements in various industries like a nuclear, power plant and chemical industries. The weld joining process and filler metal choices show the impact on the final weld joint properties. Due to the associated weld process, residual stresses play a significant role like weld distortions and mechanical properties of the joints. Dissimilar materials like SS316L and Inconel 625 plates are joined by using multipass gas tungsten arc welding process with using filler material ERNiCrMo-3 grade. The final weld joints are evaluated for residual stress measurements using X-ray diffraction technique. Thermal distributions during the welding process are mapped with Thermal imaging process in weld joints and base plate interface. Simulations of the thermal and residual stress have been carried by sequence coupled thermo-mechanical analysis using the ANSYS Parametric Design Language with double ellipsoidal heat source model with relevant material properties for both SS316L and Inconel 625 grade materials. Residual stress measurements and simulation results have shown good agreement. The details of the experiments conducted and evaluated residual stresses, modelling and comparison are described in the paper.

Keywords: Dissimilar materials, FEA, Infrared thermography, Multipass welding, XRD.

1. Introduction

Arc welding process can be used welding of the thick plate with single or multipass. GTA welding process is used among the process, which has fewer defects compared with other processes. Dissimilar materials welding has attracted owing to the stringent requirements in the industry like nuclear pressure vessels, chemical plants and aeronautical sectors. Welding of austenitic steels (SS316L) and Inconel alloy (Inconel625) have some interesting applications in nuclear, chemical and space applications.

Due to the dissimilar material grades, the weld joining process choice play an acute role on the final joint properties, hence, it is important to step for the weld process selection. The multipass welding process was carried out for SS thick jobs with both experimental and numerical analysis used to study the temperature and residual stress distribution in the weldments with 2-dimensional axisymmetric FEA [1]. Goldak et al. [2] mentioned that a numerous data is available on 3-dimensional welding simulation of similar and dissimilar welding with a suitable heat flux model for arc welding process among that double ellipsoidal heat source model is popular.

By employing finite element analysis, 3-dimensional models are developed for welding simulations using the welding process parameters effects on weld thermal temperatures and residual stresses in the butt weld joints for a single pass and multipass welding by different approaches like using the element birth and death and volumetric heat flux techniques [3-5]. Thermo-metallurgical and thermo-mechanical analysis are explored using SYSWELD for laser welding process for dissimilar welding of a thick plate of 9Cr-1Mo (V, Nb) and stainless-steel materials for residual stress study experimentally with neutron diffraction technique and simulations [6]. Interpass temperature was maintained between the pass to avoid hot cracking and to improve the microstructure and mechanical properties in the weldments [7-9]. The dissimilar welding of Inconel 657 to austenitic stainless steel 310 was characterized for thick plates of 12 mm size, the study detailed of weldability, the influence on structural properties of the weldments [10, 11]. The comparative studies of microstructure and mechanical properties of the multipass similar and dissimilar welding of Inconel to stainless steel were carried out with GTAW processes using the ERNiCrMo-3 filler wire [12, 13].

According to Kumar et al. [14], the metallurgical and mechanical properties had been studied for multipass dissimilar welds of IN625 to SS316L with different filler wires using continuous current and pulsed current GTAW process. Finite element analysis is carried out using ABAQUS with volumetric heat flux to understand the thermal distribution and leads to residual stress in the dissimilar materials [15]. The shape of plate and pipes structures are butt welded, the samples are experiments and validated with a 3-dimensional model using ANSYS and ABAQUS packages, for understanding the behaviour of temperatures, distortions and residual stress distribution in the samples [16-18]. The criticality of the weld process parameters choice is reported in detail, which causes distortion and residual stresses in multipass dissimilar joints [19]. In his report level four, (L_4) orthogonal array was used. Taguchi technique was used for optimization and concluded that pulsed current gas tungsten arc welding process was reported to have the least residual stresses compared with continuous current gas tungsten arc welding process.

Salerno et al. [20] had reported that thermal mapping and residual stress generated during multipass welding for IN718 with both experimental and simulation validation with ABAQUS and SYSWELD packages. Distortion and residual stresses developed due to the temperatures during multipass welding process of different joints in weldment [21-23]. The weld plate temperature measurement is carried out by for the weldment with thermocouples, which are placed at a various position on the top surface of the weldment. The residual stresses are measured at both the top and bottom side of the weldment.

The simulation was carried out with temperature-dependent thermo-mechanical properties of the base material. The double ellipsoidal heat source models are employed for deeper penetration investigations. The tensile residual stresses are observed and further ending with compressive stresses and stresses are self-balanced within the structure.

Due to the feeble data on the welded joints of SS316L and Inconel625, the present study has been initiated to characterize the thermal behaviour and residual stresses present in dissimilar welds. Some validation models with ANSYS Parametric Design Language. FEA models are employed for the estimation of the temperature states and residual stress in the dissimilar welded joints and are compared in both similar and dissimilar welded joint with supporting experiments.

The present paper deals with the details of experiments on the SS316L to Inconel plates GTAW process weld temperature measurements during welding by using Infrared Thermography imaging technique, residual stresses evaluation by XRD technique and the data comparison with the simulated FEA model results for residual stresses are explored.

2. Experimentation and Simulation

2.1. Weld samples fabrication procedure

SS316L and Inconel625 grades plates of dimensions 100 mm × 60 mm × 5 mm of each material are used for the weld samples fabrication. In order to join these two dissimilar materials, suitable filler wire ERNiCrMo-3 was used as it provides the best combination for the appropriate weld joint properties. The chemical composition of SS316L, Inconel625 and filler wire is given in Table 1 for reference. The base materials plates are machined with V-groove joint preparation with 60^0 as include groove angle, 2 mm root height, and 2 mm root gap and sample schematic is shown in Fig. 1 for details.

The welding procedure of the GTAW process was carried out to join these two dissimilar plates with three number of weld passes. As interpass temperature plays a critical role in final weld joint properties, it was kept around ~200 ^{0}C [19] for these experimental sample preparations. This helps in the final joint production without any hot cracks, proper microstructure formation and attaining good mechanical properties.

Proper attention and weld procedure was adapted for the good joint fabrication. The final fabricated welded sample was shown in Fig. 2 with final dimensions 200 mm × 60 mm × 5 mm and the x-ray radiography of the weld joint test was shown in Fig. 3 for reference. This confirms no presence of weld defects like cracks, porosity or micro-cracks in the welded zone.

Table 1. Composition details of Inconel625, SS316L and filler materials used.

Samples	Element (% weight)								
	Ni	**C**	**Mn**	**S**	**Cu**	**Si**	**Cr**	**P**	**Others**
Inconel 625	Min 58	Max 0.1	Max 0.5	Max 0.015	Max 0.5	Max 0.5	20-23	Max 0.015	Fe 5, Al 0.40, Mo 8-10, Ti 0.1
SS316L	App 12.00-18.00	Max 0.03	Max 2.00	Max 0.030	-	Max 1.00	16.00-18.00	Max 0.045	Mo 2-3
Filler wire									
ErNiCrMo-3	Min 64	Max 0.1	Max 0.5	Max 0.015	Max 0.50	Max 0.50	22.0-23.0	Max 0.015	Fe 1.0, Al 0.40, Nb 3.6-4.5, Mo 0.015, Ti 0.40

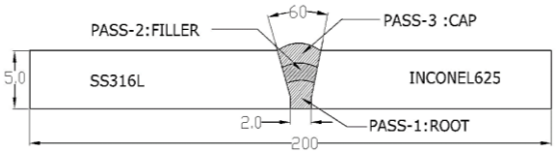

Fig. 1. Illustration of a multipass welded sample.

Fig. 2. Multipass welded sample.

Fig. 3. Radiography test results.

2.2. Measuring techniques

2.2.1. Infrared thermography

During the welding process, the weld pool temperature measurements are recorded with infrared thermography imaging throughout the welding process. The recording of temperature profiles across the welded region is measured for each pass at the specified location on the welded specimens. These values are experimentally observed and useful to the validation of the modelled thermal behaviour profiles with estimated results from the models. The temperatures were measured using the FLIR infrared thermography, with an accuracy of +/-0.1 ^{0}C. The thermal imager measures the amount of heat emitted by the surface. In order to calculate the surface temperature, it is necessary to know the surface-emission efficiency. This is referred to as emissivity are given in Eq. (1).

$$W_X = W_e + W_r + W_t \tag{1}$$

2.2.2. X-Ray diffraction

During the joining process, the fusion zone undergoes heating and cooling cycles. The heat generated is conducted to other sides of the plates, which will cause the structure to distortion and residual stresses. Residual stresses produced by existence stress even after exclusion of the exterior forces from the material. The residual stress estimation

was done out by means of the smaller focus X-ray diffraction: a Bruker D8-Discover™ system is shown in Figs. 4 and 5 demonstrate the goniometer with head, with Vantec™ area locator and suitable video in addition to laser tracking.

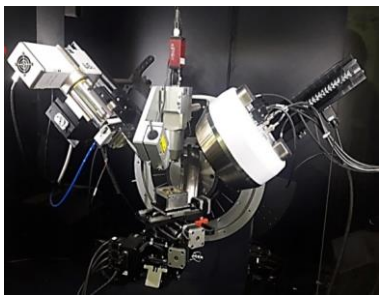

Fig. 4. Bruker x-ray diffraction.

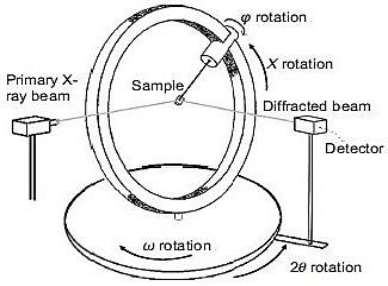

Fig. 5. Goniometer head with a detector.

The residual stress measurement in weldment is carried out using x-ray Diffraction technique by using Bragg's angle as shown in Eq. (2). Whereas *n* is the order of reflection beam, *d* is interlunar lattice spacing. The residual stress was measured on the top surface of a weldment in the transverse direction and calculation [24] of the residual stress is carried out by using the Eq. (3).

$$n\lambda = 2d\sin\theta \tag{2}$$

$$\sigma_{\phi} = \frac{m}{d_0}\left(\frac{E}{1+V}\right) \tag{3}$$

The material is in strain, the d-separating increments and when the material is in pressure, the d-dividing contracts are different because of welding parameters and rate of cooling. The residual stresses are uneven in transmission, whichever sides of the weldments because of its thermal properties.

2.3. Finite element analysis

The base materials thermal and mechanical properties [3] used for the FEA study are shown in Fig. 6. In Fig. 4(a), it shows the thermal conductivity of materials at 303 ^{0}K for SS316L is 13.36 W/m K and for Inconel625 9.8 W/m K, hence, SS316L has about 1.37 times more conductivity then Inconel, where heat is given at the joint more heat will flow toward SS316L.

The double ellipsoidal [2] heat source model was established and assigned for the GTAW process as shown in Fig. 7. Quasi-steady state heat conduction equation used for the welding process, the governing equation for the conduction process is given in Eq. (4).

$$\frac{\partial}{\partial x}\left(k\frac{\partial T}{\partial x}\right)+\frac{\partial}{\partial y}\left(k\frac{\partial T}{\partial y}\right)+\frac{\partial}{\partial z}\left(k\frac{\partial T}{\partial z}\right)+Q=-\rho C_p v\frac{\partial T}{\partial t} \tag{4}$$

where density is ρ, specific heat under constant pressure is C_p, conductivity is k of the base materials, whereas welding speed and time are V, t for the welding process. The heat input is calculated for the welding process using the equation as given in Eq. (5).

$$Q = \eta UI / V_H \tag{5}$$

where the arc welding efficiency is η, the process parameter voltage U, and I welding current amps and V_H is the volumetric heat load Watts. The heat source may be point, line, surface, flux concentrated over the surface from the centre of the arc. The a, b, c is the semi-axis of the double ellipsoidal heat source model, which are given in Eq. (6). The presented notations a, b_f, b_r and c are source fixed parameters that describe the size and profile of the ellipses, subsequently the temperature source circulation. In the given schematic, a and c denotes the double-ellipsoidal model parameters, relating to the width and depth of the fusion zone.

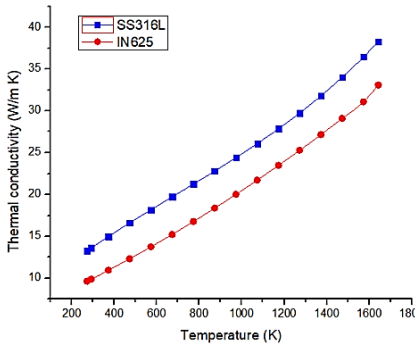

(a)Thermal conductivity of materials.

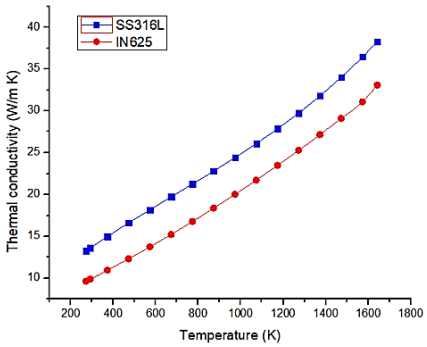

(b) Density of materials.

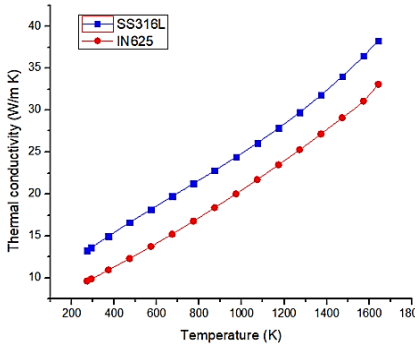

(c) Specific heat of materials.

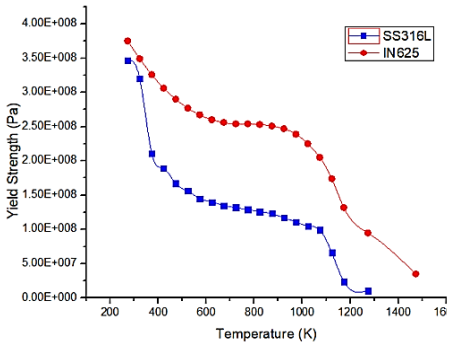

(d) Specific heat of materials.

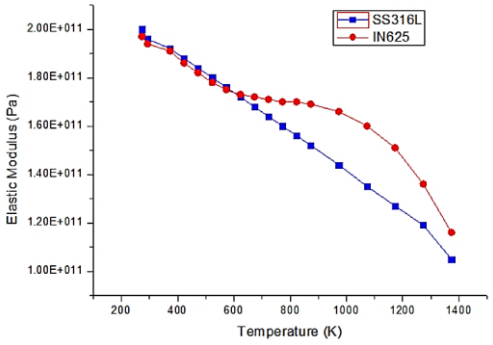

(e) Elastic modulus of materials.

Fig. 6. Thermo-mechanical properties of base materials.

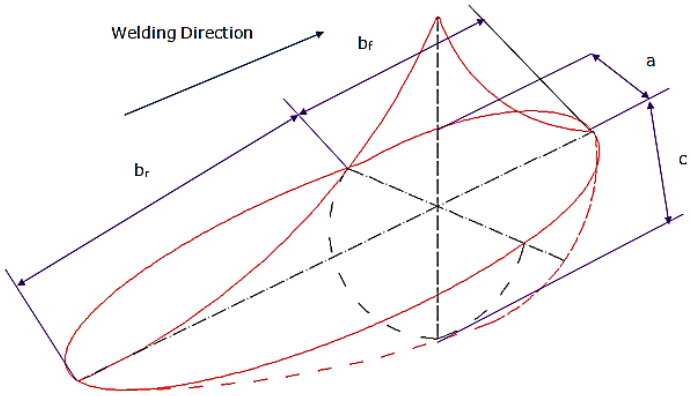

Fig. 7. Double Ellipsoidal heat flux.

$$Q(x,y,z)=\frac{6\sqrt{3}r_f\,Q}{abc\pi\sqrt{\pi}}\exp\left(-\frac{3x^2}{c^2hf}-\frac{3y^2}{a^2h}-\frac{3z^2}{b^2h}\right) \quad (6)$$

The coefficient of heat transfer rate is calculated for the weldment are given in Eq. (7). The convection is applied at the top and side faces of the weldment for the first two passes and the third pass both convection and radiation were applied on the top surface only as given in Eqs. (8) and (9). Whereas, T_0 is ambient temperature, ε is the emissivity of the base materials, σ is the Stefan-Boltzmann constant, and h is convective heat coefficient.

$$H = 24.1*10^{-4}\varepsilon T^{1.61} \quad (7)$$

$$q_C = h(T - T_0) \quad (8)$$

$$q_r = \varepsilon\sigma(T^4 - T_0^4) \quad (9)$$

The established model is adapted with the boundary conditions in order to treat the thermal behaviour of the weld passes treatment into the model. In weld pass-1, the initial temperature was the ambient temperature, then 250 ^{0}C was maintained for the remaining weld pass. First, two passes convection was applied on the surface and gat between the plates. In weld pass-3, both convection and radiation were applied on the surface.

3. Results and Discussions

3.1. Thermal history through IR thermography experiments and FEA comparison

Figures 8(a) to (c) show the temperature distribution for dissimilar weldments of SS316L to IN625, line -1(black colour) and line-2 (blue colour) represents in the transverse and longitudinal directions respectively in the graphical representation. The Y-axis represents the temperatures and X-axis represents distance on the surface of the weldment for Figs. 8(a) to (c). The maximum temperature peak was

observed at the fusion zone and when the line moves from away from the area of the incident is the temperature curve retarding to the ambient temperature.

Figure 8(a) shows weld pass-1 temperature distribution, which was varied from 1769 °C to 1884 °C and also, it was observed that the sudden increase in temperature in the 2nd peak, because of the interference of tungsten electrode and filler rod in the premises of the fusion zone. In the case of the weld pass-2 thermal profile shown in Fig. 8(b), the temperature observed varied from 1452 °C to 1942 °C. Further, Fig. 8(c) shows the weld pass-3 temperature distribution, which varies from 1790 °C to 1963 °C. The temperature distribution over the SS side is progressively decreasing along the HAZ region followed by the base plate.

Whereas, in the Inconel side the temperature distribution was decreasing at a faster rate as compared to the SS side. From this observation, it is evident that there is a divergence in the temperature distributions in the weldments due to the thermal, mechanical and structural properties of the SS316L and IN625 materials. SS316L is basically about 72% iron, 10% Nickel elements and composition-wise Inconel 625 and ERNiCrMo-3 are similar with about 5% iron, 58% Nickel.

Filler wire is more associative with Inconel625 compared to SS316L. During the welding process, the addition of filler wire in the molten state mixes homogeneously with Inconel625 and non-homogeneously with SS316L, which cause for variations in temperature and stress distributions.

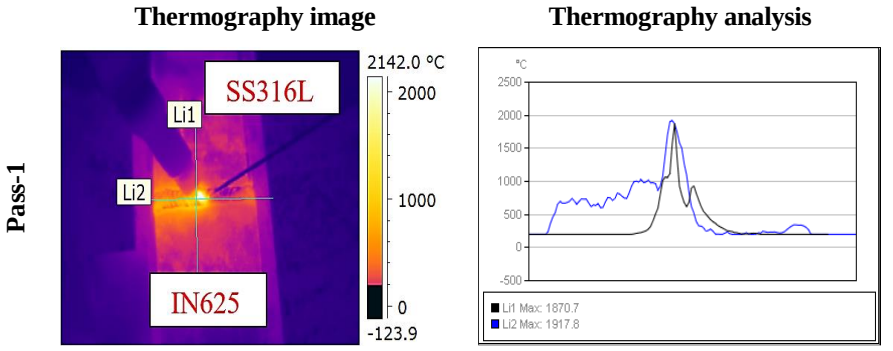

(a) Pass-1.

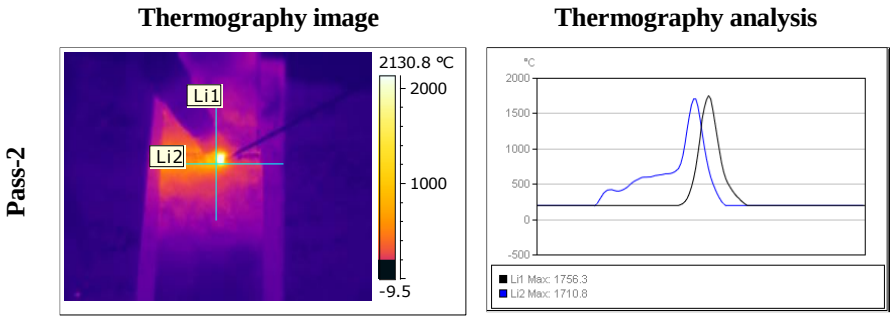

(b) Pass-2.

Thermography image **Thermography analysis**

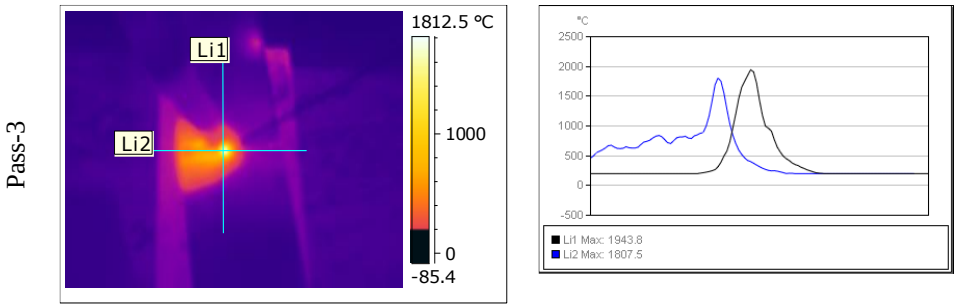

(c) Pass-3.

Fig. 8. Thermal analysis from thermography.

3.2. Simulation using FEA

The modelling of the plates and thermomechanical analysis are carried out using APDL in ANSYS package. The computer with a conflagration of Windows 7 with 8.00GB RAM, Intel(R) Core (TM), i5-8250U CPU @ 1.60GHz, 1.80 GHz used for FEA simulation. The SOLID70 element [4] were used for the analysis. Element used in FEA, which can support both coupled analyses. At the fusion zone, fine mesh and remaining meshed with 0.03 mm size as shown in Fig. 9.

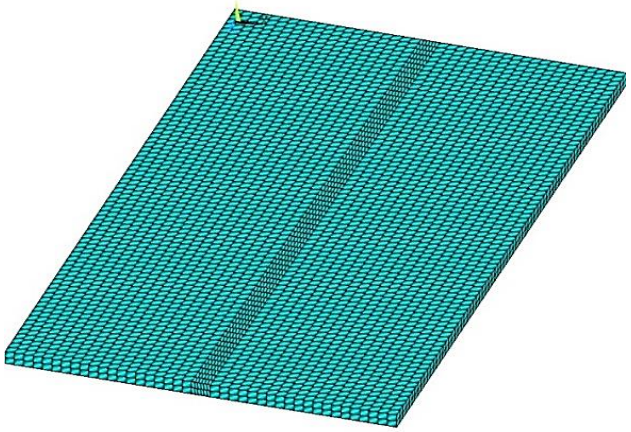

Fig. 9. Model and meshing for simulation process.

Temperature results from FEA

The welding cycle time was about 40 seconds for the thermal analysis. The cooling cycle was maintained for about 1000 seconds in between the intermediate weld passes to maintain necessary interpass temperatures. The peak temperature was observed in the fusion zone as observed in the experimental process. The heat is generated at fusion zone was distributed in all directions of the weldment. It was observed that the temperature distribution along the SS side was widespread, which attributes due to the presence of large thermal conductivity. The nodal temperature distribution of weld pass-3 is shown in Fig. 10.

Further, Fig. 11 shows the weld pass -1, sharp peak temperatures were observed at the fusion zone, the temperature was varying from an ambient temperature of 30 ^{0}C to 1700 ^{0}C. The same thermal distribution was observed in the experimentation. The HAZ temperature of both the plates was around 1150-1350 ^{0}C. For the weld pass-2, as the commencement temperature, i.e., the Interpass temperature was maintained at about 250 ^{0}C and fusion zone temperature was observed to be 1900 ^{0}C. The interpass temperature for the weld pass-3 was 230 ^{0}C, the temperature rises to 1930 ^{0}C in the fusion zone and the end of the simulation the plate edges temperature was about 200 ^{0}C. The temperature distribution for all the passes it was observed that the SS316L was experiencing high temperature as compared to the Inconel due to high thermal conductivity.

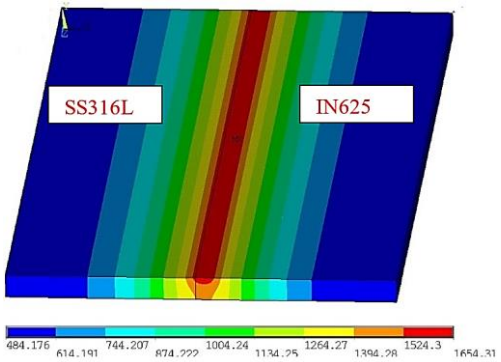

Fig. 10. Model and meshing for simulation process.

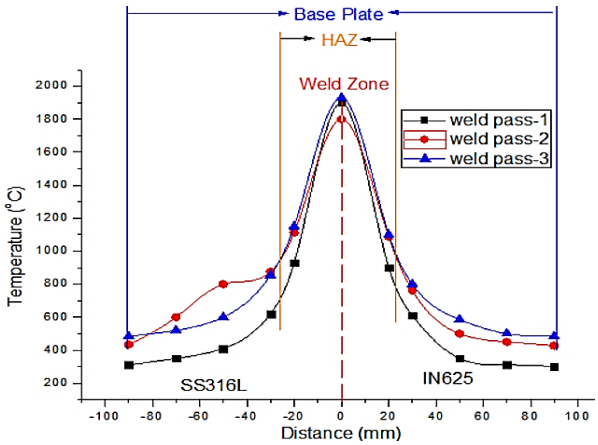

Fig. 11. Pass wise thermal distribution.

Further, in a single graph, the outcomes of the investigational, estimate of double-ellipsoidal volumetric heat sources are illustrated in Fig. 12. It is noticeable from the diagram that the results of FE simulation firmly following the experimental quantities. It is seen that the heating and cooling phases of test information are in very close concurrence with double-ellipsoidal surface heat source model.

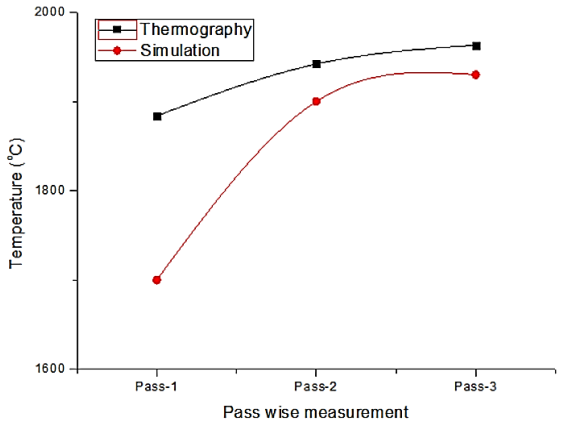

Fig. 12. Comparison of thermal distribution.

3.3. Residual stress analysis by FEA and comparison with XRD data

The sequential coupling of thermo-mechanical analysis gives the residual stresses in the numerical simulation process with a SOLID45 element. The over residual stress is shown for both experimental and simulation in Figs. 13(a) to (c). Figure 13(a) shows the weld pass-1 residual stresses, which are in tensile at fusion zone and stress decreases to compressive at HAZ of both sides of plates but SS316L experiences more compressive for the smaller area near FZ compared to Inconel. In weld pass-2, the residual stress is tensile of 30 MPa and both HAZ are also in tensile with a difference of 20 MPa and also the plates experience compressive near the end of the base plates as shown in Fig. 13(b). Similarly, Fig. 13(c) shows the results for weld pass-3, Inconel plate experiences tensile stresses and the SS plate experiences compressive stresses.

The experimental and simulated residual stress distribution are compared are shown in Fig. 14. The observed residual stress spreading is caused due to heating and cooling between the plates. The residual stress profile displayed tensile in the premises of the fusion zone and compressive stresses [18] far from it. The residual stress distribution is high in the fusion zone of the order of 180 MPa and 169 MPa in experimental and simulation respectively.

It has been observed by Vemanaboina et al. [19] that the Inconel625 has experiences tensile stress when compared with the SS316L in the HAZ the same trend has been observed in simulation analysis too. This action may attribute due to the variance in thermal and mechanical properties of the base metals. The weld zone near the SS side experiences rapid solidification and shrinkage of the metal due to SS has high thermal conductivity and thermal expansion among both the plates. From both experimental and numerical analysis, it has been observed that residual stresses were well maintained below the yield stresses of individual plates.

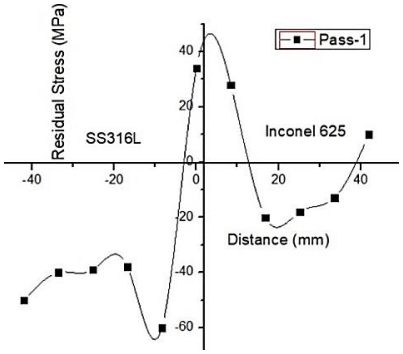

(a) Residual stress in pass-1.

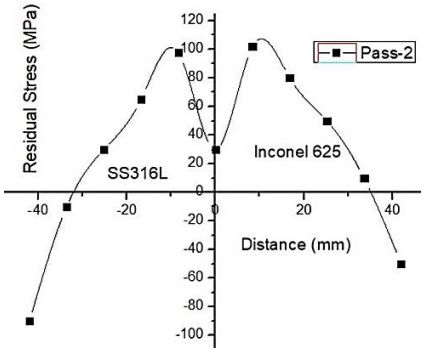

(b) Residual stress in pass-2.

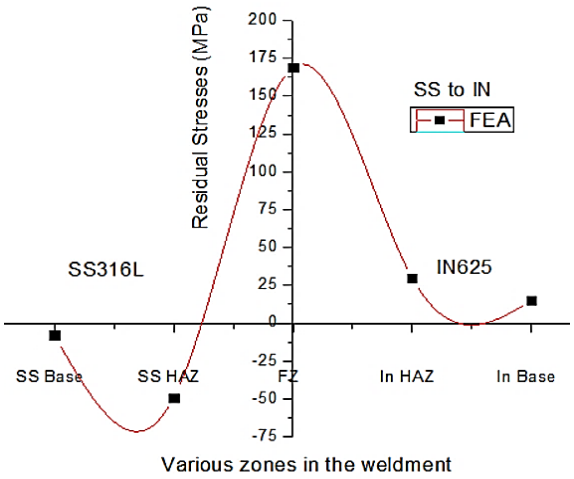

(c) Residual stress in pass-3.

Fig. 13. Residual stress distributions using FEA.

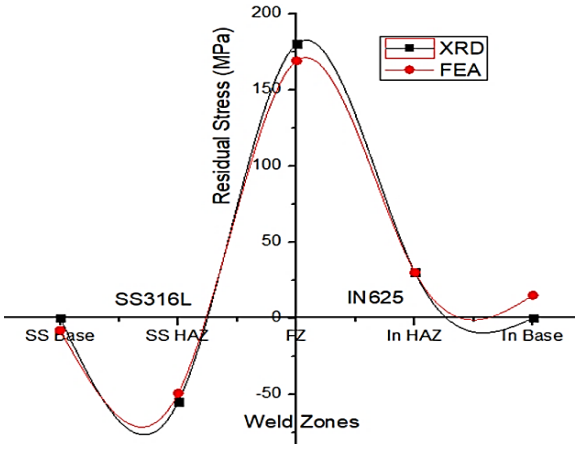

Fig. 14. Comparison of residual stress on the weldment.

4. Conclusions

The dissimilar multipass welding of SS316L to Inconel625 with GTAW process has been carried out. Defects free multipass welding by GTAW process of 5 mm thickness samples were obtained as verified by X-ray radiography test. The fusion zone temperatures and residual stress are experimentally measured with infrared thermography and x-ray diffraction techniques. FEA simulation analysis has been carried out with double ellipsoidal heat flux model developed for the GTAW. Weld thermal behaviour and residual stresses evaluation by using materials properties database carried out. The peak temperatures at weld zone as measured by infrared thermography were about 1900 ^{0}C and simulated values by the FEA model are found in a range of 1800 ^{0}C, which shows a variation of about 5%. In the case of residual stresses, the XRD compared with simulated ANSYS results had up to 10% variations. In the SS316L plate, HAZ and fusion zone have shown the compressive residual stresses whereas, in case of Inconel625, tensile stresses are observed in HAZ and fusion zone. The stresses developed in the welded structure well lie within the structure. The residual stresses generated are within the yield limits of the materials. The factor of safety was 1.38 for SS316L and 1.14 for Inconel625.

Nomenclatures

c	Specific heat, J/kg K
H	Convective heat transfer coefficient, W/m^2 K
K_m	Thermal conductivity, W/m^2 K
Q	Energy input rate, W
q_L	Heat flux of laser process
q_t	Heat flux of TIG process
r	Material density, kg/m^3
T	Temperature, K

Greek Symbols

ε	Emissivity

Abbreviations

APDL	ANSYS Parametric Design Language
FEA	Finite Element Analysis
FEM	Finite Element Method
FLIR	Forward-Looking Infrared
FZ	Fusion Zone
GTAW	Gas Tungsten Arc Welding
HAZ	Heat Affected Zone
SS	Stainless Steel
XRD	X-Ray Diffraction

References

1. Deng, D.; Murakawa, H.; and Liang, W. (2008). Numerical and experimental investigations on welding residual stress in multi-pass butt-welded austenitic stainless-steel pipe. *Computational Materials Science*, 42(2), 234-244.

2. Goldak, J.; Chakravarti, A.; and Bibby, M. (1984). A new finite element model for welding heat sources. *Metallurgical Transactions B*, 15(2), 299-305.
3. Capriccioli, A.; and Frosi, P. (2009). Multipurpose ANSYS FE procedure for welding processes simulation. *Fusion Engineering and Design*, 84(2-6), 546-553.
4. Vemanaboina, H.; Akella, S.; and Buddu, R.K. (2014). Welding process simulation model for temperature and residual stress analysis. *Procedia Materials Science*, 6, 1539-1546.
5. Akella, M.S.; Harinadh, V.; Krishna, Y.; and Buddu, R.K. (2014). A welding simulation of dissimilar materials SS304 and copper. *Procedia Materials Science*, 5, 2440-2449.
6. Kumar, S.; Awasthi, R.; Viswanadham, C.S.; Bhanumurthy, K.; and Dey, G.K. (2014). Thermo-metallurgical and thermo-mechanical computations for laser welded joint in 9Cr-1Mo (V, Nb) ferritic/martensitic steel. *Materials and Design*, 59, 211-220.
7. Murugan, S.; Rai, S.K.; Kumar, P.V.; Jayakumar, T.; Raj, B.; and Bose, M.S.C. (2001). Temperature distribution and residual stresses due to multipass welding in type 304 stainless steel and low carbon steel weld pads. *International Journal of Pressure Vessels and Piping*, 78(4), 307-317.
8. Buddu, R.K.; Chauhan, N.; and Raole, P.M. (2014). Mechanical properties and microstructural investigations of TIG welded 40 mm and 60 mm thick SS 316L samples for fusion reactor vacuum vessel applications. *Fusion Engineering and Design*, 89(12), 3149-3158.
9. Buddu, R.K.; Chauhan, N.L.; and Raole, P.M. (2014). Investigations of microstructure and mechanical properties of 60-mm-thick type 316L stainless steel welded plates by multipass tungsten inert gas welding and electron beam welding for fusion reactor applications. *Fusion Science and Technology*, 65(2), 248-254.
10. Naffakh, H.; Shamanian, M.; and Ashrafizadeh, F. (2008). Weldability in dissimilar welds between Type 310 austenitic stainless steel and alloy 657. *Journal of Materials Science*, 43(15), 5300-5304.
11. Naffakh, H.; Shamanian, M.; and Ashrafizadeh, F. (2008). Influence of artificial aging on microstructure and mechanical properties of dissimilar welds between 310 stainless steel and INCONEL 657. *Metallurgical and Materials Transactions A*, 39(10), 2403-2415.
12. Harinadh, V.; Edison, G.; Akella, S.; Reddy, L.S.; and Buddu, R.K. (2017). Multipass welding on inconel material with pulsed current gas tungsten arc welding. *Materials Today: Proceedings*, 4(2), Part A, 1452-1458.
13. Ramkumar, K.D.; Mithilesh, P.; Varun, D.; Reddy, A.R.G.; Arivazhagan, N.; Narayanan, S.; and Kumar, K.G. (2014). Characterization of microstructure and mechanical properties of Inconel 625 and AISI 304 Dissimilar Weldments. *ISIJ International*, 54(4), 900-908.
14. Kumar, K.G.; Ramkumar, K.D.; and Arivazhagan, N. (2015). Characterization of metallurgical and mechanical properties on the multi-pass welding of Inconel 625 and AISI 316L. *Journal of Mechanical Science and Technology*, 29(3), 1039-1047.

15. Ebrahimi, A.N.; Arab, N.B.M.; and Gollo, M.H. (2015). Thermal analysis of laser beam welding of nickel-based super alloy Inconel 625 to AISI 316L, using gaussian optics theory in keyhole. *Journal of the Brazilian Society of Mechanical Sciences and Engineering*, 38(4), 1199-1206.
16. Zubairuddin, M.; Albert, S.K.; Mahadevan, S.; Vasudevan, M.; Chaudhari, V.; and Suri, V.K. (2014). Experimental and finite element analysis of residual stress and distortion in GTA welding of modified 9Cr-1Mo steel. *Journal of Mechanical Science and Technology*, 28(12), 5095-5105.
17. Lee, K.; Kim, M.; and Lee, S. (2013). Three-dimensional finite element analysis for estimation of the weld residual stress in the dissimilar butt weld piping. *Journal of Mechanical Science and Technology*, 27(1), 57-62.
18. Venkatkumar, D.; and Ravindran, D. (2016). 3D finite element simulation of temperature distribution, residual stress and distortion on 304 stainless steel plates using GTA welding. *Journal of Mechanical Science and Technology*, 30(1), 67-76.
19. Vemanaboina, H.; Edison, G.; and Akella, S. (2018). Effect of residual stresses of GTA welding for dissimilar materials. *Materials Research*, 21(4), 8 pages.
20. Salerno, G.; Bennett, C.; Sun, W.; Becker, A.; Palumbo, N.; Kelleher, J.; and Zhang, S.Y. (2018). On the interaction between welding residual stresses: A numerical and experimental investigation. *International Journal of Mechanical Sciences*; 144, 654-667.
21. Park, J.-u.; An, G.; and Woo, W. (2018). The effect of initial stress induced during the steel manufacturing process on the welding residual stress in multi-pass butt welding. *International Journal of Naval Architecture and Ocean Engineering*, 10(2), 129-140.
22. Genchev, G.; Doynov, N.; Ossenbrink, R.; Michailov, V.; Bokuchava, G.; and Petrov, P. (2017). Residual stresses formation in multi-pass weldment: A numerical and experimental study. *Journal of Constructional Steel Research*, 138, 633-641.
23. Kartal M.E.; Kang Y.-H.; Korsunsky A.M.; Cocks A.C.F.; and Bouchard J.P. (2016). The influence of welding procedure and plate geometry on residual stresses in thick components. *International Journal of Solids and Structures*, 80, 420-429.
24. Anderoglu, O. (2004) *Residual stress measurement using x-ray diffraction.* Master Thesis. Texas A & M University, Texas, United States of America.